fluids

MDPI

Article

Optimization of the Circular Experimental Channel for PIV Measurements of Internal Aerodynamic Cases

Jaroslav Pulec, Petra Dančová * and Jan Novosád

Department of Power Engineering Equipment, Faculty of Mechanical Engineering, TU Liberec, Studentská 2, 46117 Liberec, Czech Republic

* Correspondence: petra.dancova@tul.cz

Abstract: This paper deals with the design of an experimental circular channel model specially adapted for particle image velocimetry (PIV) measurements of airflow. The goal is to find a simple, fast, and functional approach for creating experimental models. The issue of the required PIV signal quality is defined, and the limits of acquiring relevant PIV data in the interior of circular channels are described, primarily as reflections of direct and scattered laser light caused by light passage through the cylindrical wall. As part of the experiment, measurements of reflections were made on differently coated surfaces of a plexiglass plate. Samples of various combinations of black matt spray, Rhodamine 6G coating, and roughened surface were created. From the presented results, a combination of black matt spray with a layer of Rhodamine 6G spray paint was chosen. The selected modification was further used for the internal modification of the experimental channel surface. Furthermore, a geometry modification to prevent light spread through the tube material is described. Data obtained from measurements before and after channel modification are presented and explained.

Keywords: particle image velocimetry; circular pipe; unfavorable reflection prevention; surface finishes; geometry modifications

check for updates

Citation: Pulec, J.; Dančová, P.; Novosád, J. Optimization of the Circular Experimental Channel for PIV Measurements of Internal Aerodynamic Cases. *Fluids* **2023**, *8*, 62. https://doi.org/10.3390/fluids8020062

Academic Editors: Pier Marzocca and Mehrdad Massoudi

Received: 7 December 2022
Revised: 19 January 2023
Accepted: 8 February 2023
Published: 10 February 2023

Copyright: © 2023 by the authors. Licensee MDPI, Basel, Switzerland. This article is an open access article distributed under the terms and conditions of the Creative Commons Attribution (CC BY) license (https://creativecommons.org/licenses/by/4.0/).

1. Introduction

Particle image velocimetry (PIV) is an optical method for velocity field measurement. The principle of the technique is the pulsed illumination of tracer particles from which velocity vectors are calculated in sub-regions called interrogation windows according to the change in particle positions between exposures [1,2]. Illumination is usually performed with a laser that creates an illuminated plane: planar and stereoscopic PIV [3] or volume: 3D PIV [4]. The acquired data must have a sufficient signal-to-noise ratio (SNR) [5]. The favorable SNR requires a unique approach to prepare the experimental model so that the light scattered by tracer particles has the highest light intensity on the recording and negative optical phenomena such as reflection and refraction are eliminated. There is also a risk of camera sensor damage due to the high intensity of the reflected light [6].

Wieneke [7] explained several sources of uncertainty generated in the data acquisition process that decrease the SNR, for example, timing and synchronization errors, perspective errors, camera noise, etc. Xue et al. [5] described a quantification of PIV measurement uncertainty directly from the information in the cross-correlation plane, i.e., the correlation plane obtained from the double frame mode record. The cross-correlation plane is the distribution of probabilities for image pattern displacement in the interrogation window. On the horizontal axes, there are coordinates of the interrogation window in pixels. The vertical axis represents signal and noise strength. In every interrogation window, only one primary peak represents the signal strength, and its position within the evaluated square determines the size and direction of the flow velocity vector. There are also many smaller

peaks representing unwanted digital and optical noise. The basic way to determine the SNR is the primary peak ratio (PPR) method [8]:

$$\mathrm{PPR} = \frac{c_{\max}}{c_2}, \tag{1}$$

where $c_{\max}$ is the primary peak height and c_2 is the height of the second-highest peak. The PPR of ideal data approaches infinity. Conversely, if the cross-correlation plane contains only noise, the PPR equals one. For quality results, the primary peak must have sufficient height separation from the noise and adequate width of the primary peak. It can be achieved using an appropriate experimental setup, correct saturation density of tracer particles, and appropriately chosen digital corrections of image data.

The method of illumination of the measuring plane must be taken into account. If the geometry arrangement does not allow the position of the laser sheet source axially, then it is necessary to illuminate the cylindrical experimental chamber radially. However, passing laser light through the cylindrical wall brings many complications, e.g., reflections and scattering. At both interfaces between the transparent cylindrical wall and air, the laser beams are refracted and transmitted through the internal structure of the wall to unwanted locations. Kong et al. [9] published a study of light beam transmission through a cylindrical wall. As Figure 1 shows, the incident beam perpendicular to the axis of the pipe is divided into a reflection part and a transmission part at the interfaces of a hollow cylinder of inner radius r_1 and outer radius r_2. There is an assumption of wall refractive index n_2 and refractive index of the environment outside wall n_1. The angles of incidence θ_i, reflection $\theta_\mathrm{f,}$ and refraction θ_t at the first interface are also shown.

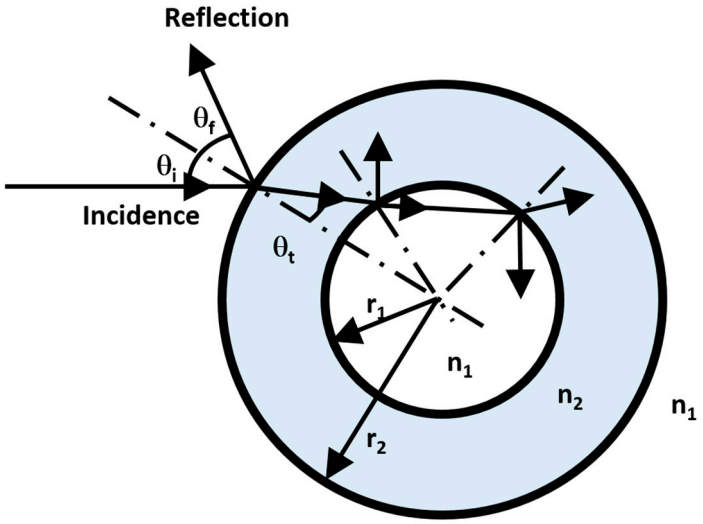


Figure 1. Scheme of ray tracing in the transparent cylindrical pipe.

In [9], Kong measured and calculated the intensity of diffused light around the circumference of the pipe in polar coordinates. In the case of incidence, the angle $\theta_\mathrm{i} = 0°$, and the data showed the clearly readable central peak between -30 and 30 degrees caused by the direct passage of the laser beam through all interfaces. There is also a secondary peak region in $\pm(35 \div 60)°$. This effect can adversely affect the quality of PIV data and needs to be eliminated.

A solution that partially eliminates negative optical effects is to subtract the unchanging background from the measured data. This software solution is helpful for the accurate calculation of the vector fields but is often insufficient because it does not eliminate the amount of light incident on the camera sensor. This light can be destructive to the sensor. A detailed description of this pre-processing method has been discussed, for example, by Adatrao and Sciacchitano [10], Theunissen et al. [11], and Deen et al. [12].

Using a similarity theory is a suitable method to replace the gas medium with liquid. A liquid medium allows the use of PMMA particles with the fluorescent dye Rhodamine B designed for the micro-PIV application. A camera with a suitable optical filter then records only the wavelength that the particles emit, which was used by Lindken [13], for example. Due to the high cost of the particles, Warjito et al. [14] investigated alternative particles made of resin and Rhodamine B. However, replacing gas with liquid brings other problems. In addition to the increased demands on the tightness of the track, there is high refraction of light during the transition from a gaseous environment to a liquid medium, and it causes significant distortion of the acquired data. Efforts for its elimination led to the use of optical prisms. In the case of a circular pipe, this means embedding the channel in a flooded block, such as in the works of He et al. [15], Wang et al. [16], or Chang et al. [17].

The way that the reflection can be significantly reduced is generally by using the appropriate choice of materials and coatings. Depardon et al. [18], in their study of a flat-plate boundary layer, have used a fluorescent paint based on Rhodamine 6G. In the reflection from the wall, there is then a reduced intensity in the wavelength of the laser light. Paterna et al. [6] then investigated the influence of other coatings and materials. Bisel et al. [19] demonstrated the positive effect of Rhodamine 6G coating on the 3D PIV experiment.

Recently, a paper by Novosád et al. [20] was published to verify the applicability of the PIV method for measurements in a DN 80 circular pipe as a part of the currently developed ultrasonic gas meter. This experimental model was based on the inner gas meter channel geometry, which consists of a system of straight pipes, elbows, and flow conditioning segments. The innovative geometry was designed to ensure suitable conditions for ultrasonic measurement in the straight pipe, especially the stability of the velocity profile. PIV measurements have been used for the validation of the velocity profile. The target area was made of straight plexiglass pipe with some but insufficient modifications. The inner backside from the PIV camera view was just taped over with a black matt film. An adjustable aperture blocked the adverse reflections. This measuring arrangement showed significant limitations because the measurable cross-section had thus been considerably reduced.

A very similar issue was recently solved by Wangxu et al. [21]. They measured natural gas flow in a DN 100 straight pipeline using 2D PIV. They chose to coat the inside away from the camera with black matt spraying. This modification produced better results than the foil in the previous case, but there was still a large influence of scattered light.

This study aims to develop an efficient methodology for designing and manufacturing circular experimental channels for various applications of internal aerodynamics measurements. The main goal is to improve the methods for experiment preparation used previously [20]. The work includes surface sample measurements and a subsequent PIV experiment in a circular pipe.

2. Methods

The PIV system by LaVision company with all apparatus for recording 2D PIV data was used for all experiments. The system has the following specifications:

- FlowMaster system by LaVision.
- A 5.5 MPx camera LaVision Imager sCMOS CLHS, resolution (2560 × 2160) pixels, 16 bit, a minimum time interval of two frames 120 ns, exposure time 15 µs to 100 ms, spectral range 370 nm to 1100 nm, maximum frame rate 50 Hz.
- Band-pass camera filters of 532 nm, bandwidth 10 nm.
- Nd: YAG double-cavity laser Quantel EverGreen HP, 340 mJ per pulse, wavelength 532 nm, maximum repetition frequency 15 Hz, pulse duration up to 10 nm, class 4 laser.
- LaVision Laser Guiding Arm with a system of seven mirrors, 1.5 m long.
- LaVision Sheet Optics (divergent), sheet thickness 0.5–2.5 mm, divergence lenses f = −20 mm and–10 mm, working distance 300–2000 mm.
- Optical table Newport M-VIS3672-SG4-325N, 900 × 1800 × 110 mm.

- One PC for recording and evaluation, one independent PC for evaluation, Windows 10, DaVis 10.2 software with package FlowMaster for 2D and stereoscopic PIV.
- Seeder LaVision Aerosol Generator producing 1 µm diameter droplets of Di-Ethyl-Hexyl-Sebacat (DEHS).

3. Experimental Setup for Measurement of Surface Finish Samples

Before measuring the velocity fields, the effectiveness of some surface modifications was verified. The main goal was to investigate the influence of Rhodamine 6G on reducing laser-wavelength reflections that may reduce the quality of the PIV signal. Fluorescent paint based on Rhodamine 6G was prepared by dissolution of 3 g Rhodamine 6G in 10 mL ethanol mixed with 500 mL transparent water-soluble acrylic paint. The paint was applied with a brush. There is a list of samples in Table 1. There are three samples (1, 2, 4) with standard surface modifications. The Rhodamine 6G paint was also applied as a top layer on samples 3 and 5. A sample plate is shown in Figure 2.

Table 1. List of samples.

Sample Identification	Description of Sample
1	Black matt spraying
2	Pure transparent plexiglass
3a	Black matt spraying + Rhodamine 6G coating
3b	Black matt spraying + Rhodamine 6G coating, roughened
4	Black matt foil
5a	Rhodamine 6G coating
5b	Rhodamine 6G coating, roughened



Figure 2. Plexiglass plate with various surface finishes (labels according to Table 1).

These samples were illuminated with a laser sheet, and the images of the sample plate surface were recorded using the camera with a 532 nm band-pass filter with a bandwidth of 10 nm to avoid wavelength detection outside this range. Figure 3 shows the arrangement for measuring the samples. There is a 532 nm laser that creates the laser sheet. The laser light incidences the inclined samples plate, and the light is reflected into the camera lens. The camera records the image as an intensity field.

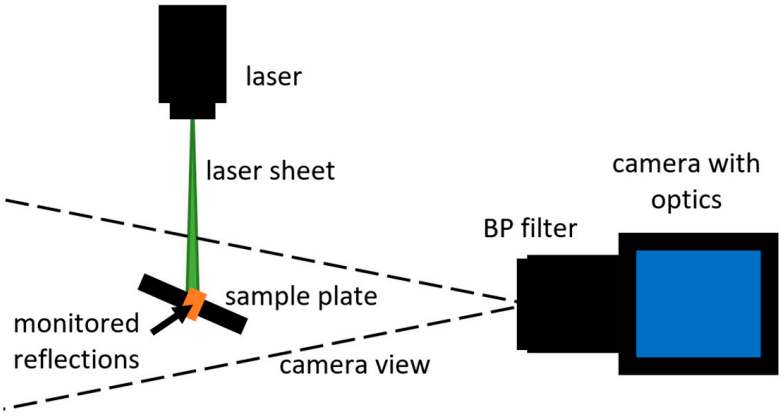


Figure 3. Samples measurement setup.

4. Results of Surface Finish Samples Measurement

In Figure 4, you can see a graph of intensity along the sample plate. The red curve symbolizes values of light intensity obtained from the average values between the red dashed lines. Peaks with values above 45,000 are reflections of the sample plate's dividing marks. Above the values of each sample, the average intensity value is shown in a rectangle. It can be noticed that samples 1, 2, 3a, and 5a have the lowest value of reflected light. Samples 3b, 4, and 5b have a significantly higher value.

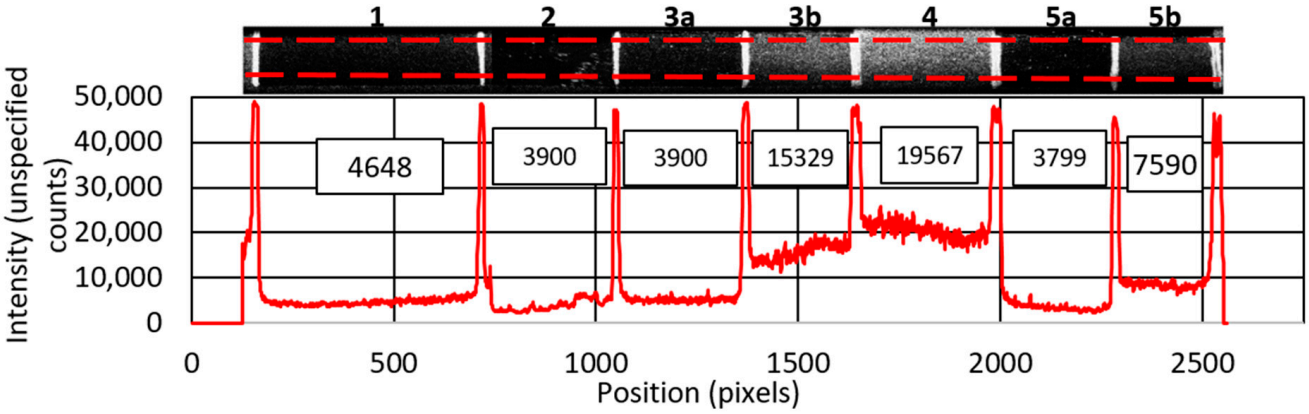


Figure 4. Light intensity waveform.

Sample 2, which corresponds to plexiglass without modification, has the most reduced intensity of reflections. This is due to the fact that most of the rays pass through the material. However, it should be noted that the sample plate is planar, not cylindrical. Because of the optical properties of the circular pipe mentioned in the introduction, it is, therefore, advisable to choose a surface modification that prevents the laser from passing through. Samples 5a and 5b present a similar problem because the coating is partially transparent. Sample 1, i.e., black matt spraying, is more favorable than sample 3a (the average intensity is 12% lower). However, for samples 3 and 5, it can be noticed that part b, with the roughened surface, has a significantly higher intensity than part a, which is also rough due to the technique of applying the dye with a brush. Thus, the brush application is not a suitable approach. Due to the behavior of the individual layers, a combination of black matt and Rhodamine 6G spray was chosen as the most favorable option.

5. Experimental Setup of the PIV Experiment

Figure 5 depicts a scheme of the experimental arrangement for PIV measurement in the straight, circular pipe. The experimental segment is made of plexiglass with an inner diameter of 80 mm and a wall thickness of 5 mm. The tube is illuminated with a laser sheet in the horizontal dividing plane. A camera with optics and a band-pass filter is placed above and scans the experimental area perpendicular to the laser sheet.

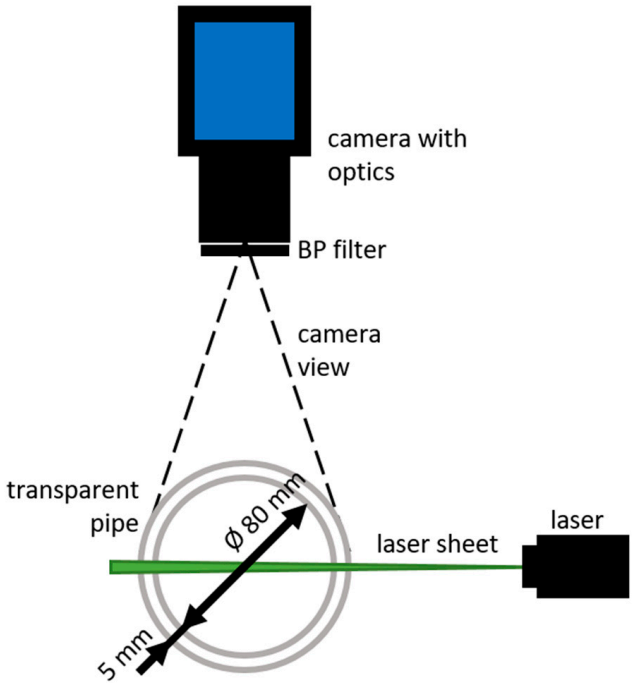


Figure 5. Experimental setup for 2D PIV measurement.

5.1. Calibration

The camera is calibrated with a flat calibration target. It is a 78 mm by 200 mm plate with 2 mm white round markers on a black background. There are 20 markers in a row and 51 markers in columns with a spacing of 3.9 mm. The calibrated area covers 74.1 mm of the pipe diameter. Only 2.95 mm close to the wall on both sides is, therefore, a non-valid measurement, which is 7.4% of the diameter. The calibration plate was created using laser printing on film. Due to the strong radial distortion on the pipe walls, a 3rd order polynomial mapping function was chosen.

5.2. Channel Modifications

First, comparative measurements were made in a duct without geometric modifications, with only a black matt film on the inside of the duct, as seen in Figure 6. Between the camera and the laser sheet, an adjustable aperture was placed as the shield against strong reflections near the walls.

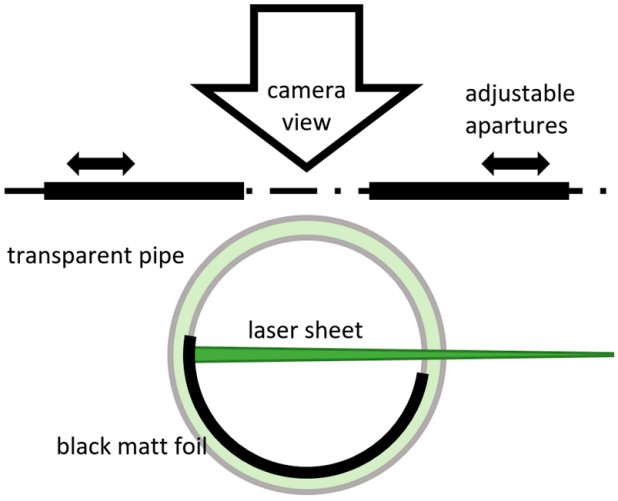


Figure 6. Comparative measurement setup.

Final measurements were made with internal black and Rhodamine 6G dye spraying and geometry modification. In Figure 7, all improvements are illustrated. An elongated 7 mm gap was cut in the area of the laser sheet passage inside the measured area, into which a 5 mm strip of flat plexiglass was inserted. Layers of black aquarium sealant avoid the light spreading into the cylindrical wall. This modification only reduces the cross-section of the channel by less than 0.02% and its inner radius by only 0.38%. A negligible influence on the nature of the flow can, therefore, be assumed.

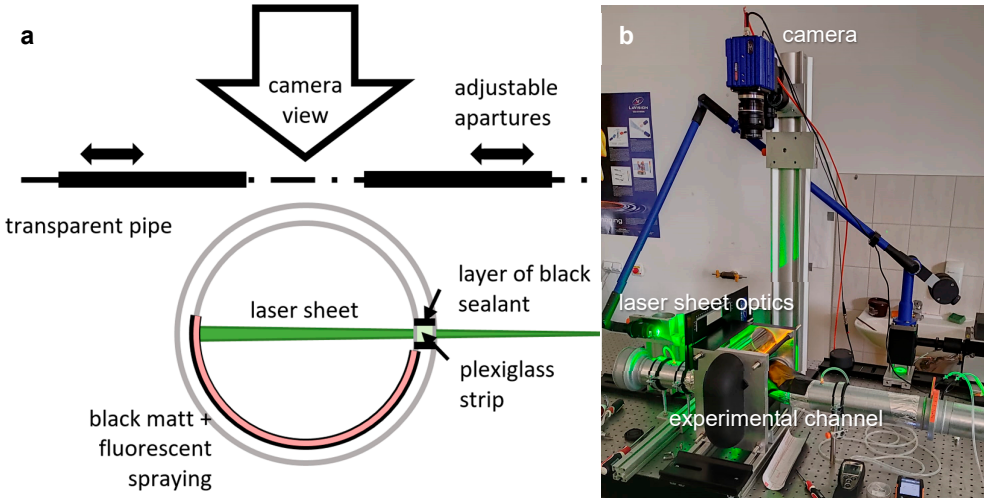


Figure 7. Scheme (**a**) and photo (**b**) of measurement in modified tube.

6. Results and Discussion

This section describes the results obtained. Six regimes were recorded, which are described in Table 2. Modes marked with 0 represent photographic data without seeding particles showing local reflections in the unmodified mode, as shown in Figure 6. The letter after the number distinguishes different degrees of shielding. Modes 1, 2, and 3 are PIV shots with varying degrees of shading and eventual pre-processing subtracting the permanent background from the image and increasing the contrast between the particle image and its surroundings. It is a good practice to complete individual subtraction for each data set because of possible variable conditions between collections, for example, changing light conditions around the experiment. Measurements of modes 1 to 3 were carried out under the same flow conditions, only with the substitution of a straight, circular part.

Table 2. List of regimes.

Regime Identification	Modification	Shielding	Background Subtraction	Seeding Particles
0a	Black matt foil	No	No	No
0b	Black matt foil	Partially	No	No
0c	Black matt foil	All reflections	No	No
1	Black matt foil	All reflections	No	Yes
2	Black matt foil	All reflections	Yes	Yes
3	Black matt + fluorescent paint spraying	No	No	Yes

In Figure 8, you can see the intensity map of regime 0a. Yellow rectangles define the boundaries of the pipe. Figure 8a displays a range of intensities from 300 to 1700 units. Figure 8b shows the full range from 0 to the sensor maximum (65,000 counts). It is possible

to notice that a small area inside the measured space attacks the maximum allowed intensity even at the lowest adjustable laser power. These two small oval reflections are probably due to the phenomenon refereed by Kong et al. [9]. Such values can only be recorded for a very short time. Otherwise, the sensor may be destroyed. Figure 9 represents regime 0b; only near-wall reflections are covered, and inside the measurement, area reflections are still there. These areas must be shielded in the current arrangement; see regime 0c in Figure 10. In this picture, both areas adjacent to the wall are covered.

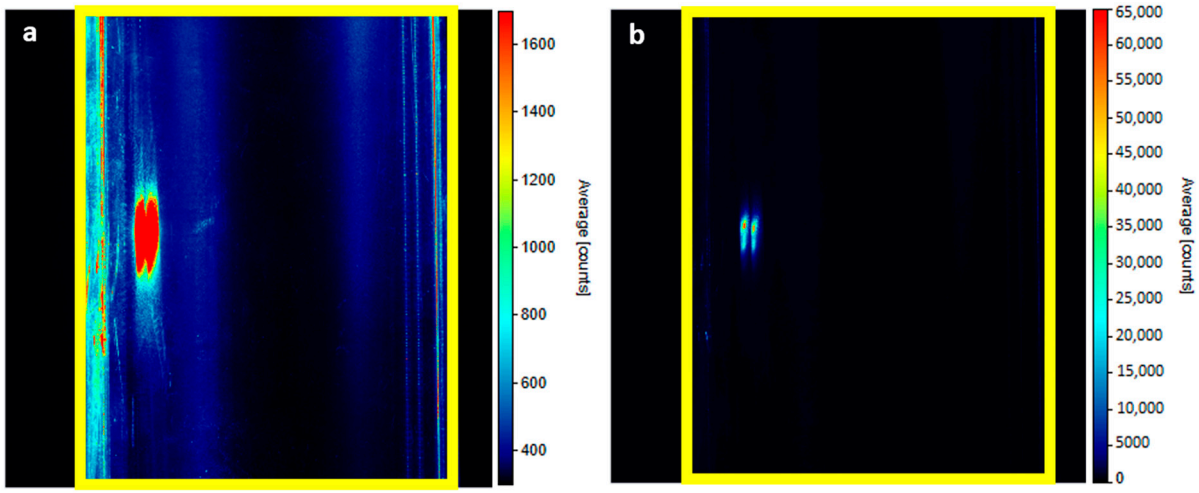


Figure 8. Regime 0a: Pipe reflections without seeding particles. (**a**) Intensity scale from 300 to 1700 counts and (**b**) full intensity range.

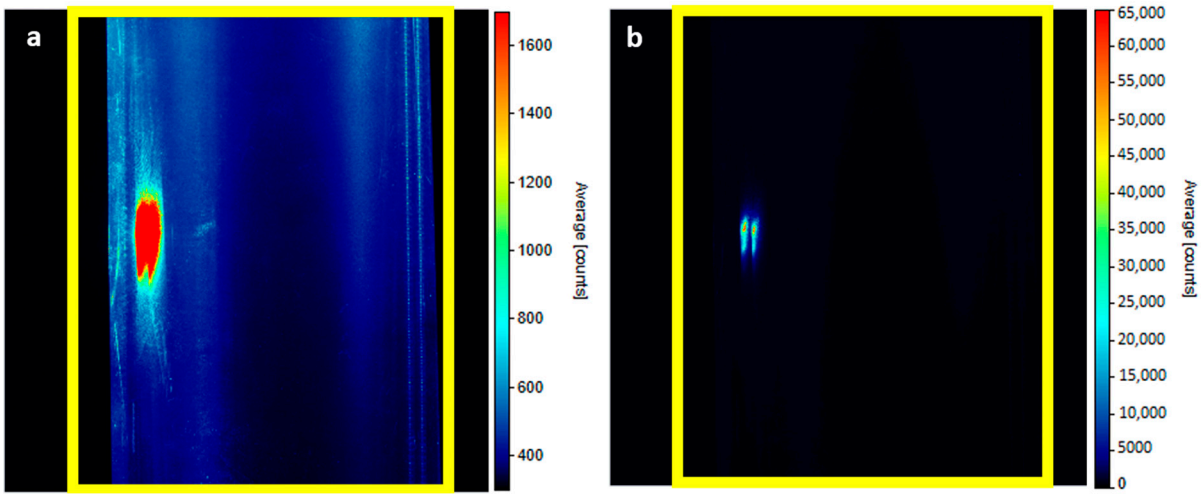


Figure 9. Regime 0b: Pipe partially covered by adjustable aperture without seeding. (**a**) Intensity scale from 300 to 1700 counts and (**b**) full intensity range.

Figure 11 shows the waveform of intensity across the channel diameter in the region of the highest reflections. The intensity axis is plotted on a logarithmic scale due to the high gradients. The graph shows the intensity of regimes 0a, 0b, and 0c, and the recorded intensity value is displayed in the area of the three highest peaks. Regimes 0a and 0b are degraded by the area where the intensity attacks the maximum of the camera sensor. Mode 0c visibly displays a shading area close to the 20 mm diameter value. The maximum intensity is 643 counts, which is less than 1% of the maximum measurable value of the sensor. However, this arrangement severely limits the measurable diameter, and moreover, the measured region is still irregularly illuminated by scattered light, which can reduce the contrast between the particles and the background, especially at higher laser power.

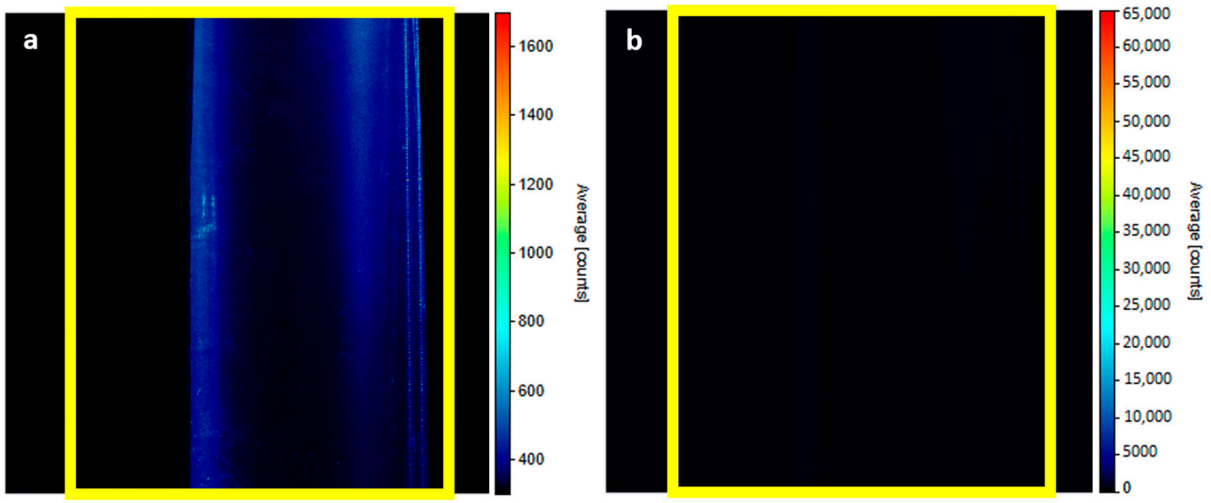


Figure 10. Regime 0c: Pipe fully covered by adjustable aperture without seeding. (**a**) Intensity scale from 300 to 1700 counts and(**b**) full intensity range.

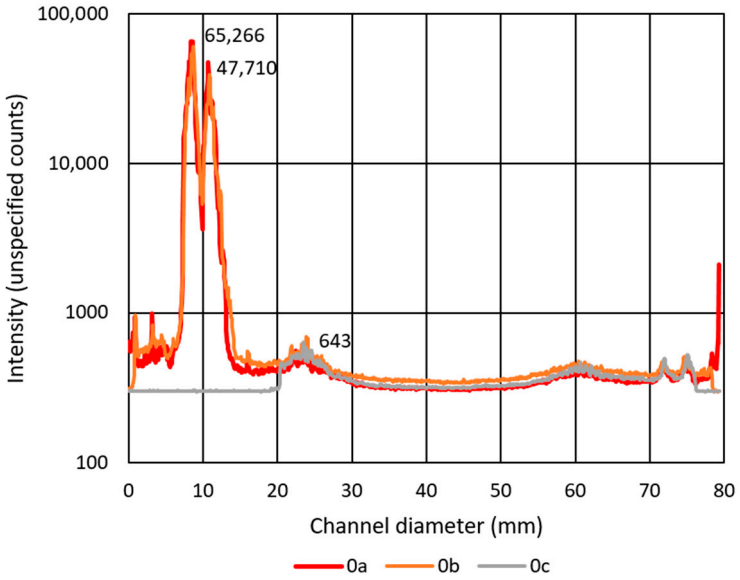


Figure 11. Intensity waveform along the diameter in the area of the highest reflections for regimes 0a, 0b, and 0c.

Sample intensity maps of the seeded channels are shown in Figure 12. These include regimes 1, 2, and 3, according to Table 2. Cases 1 and 2 are shielded due to reflections, whereas case 3 is not. It can also be seen that in case 1, the particles are not contrasted enough, so a background subtraction is necessary. On the other hand, mode 3, the modified case, allows the measurement over the whole diameter and does not even require background subtraction.

PPR analysis was performed according to Equation (1). The values of the PPR of measured regimes are written in Table 3. It can be seen that subtracting the background will contribute to a higher PPR by 0.2. Mechanical modifications of the channel lead to a further increase. It can be assumed that subtracting the background would increase this value even more.

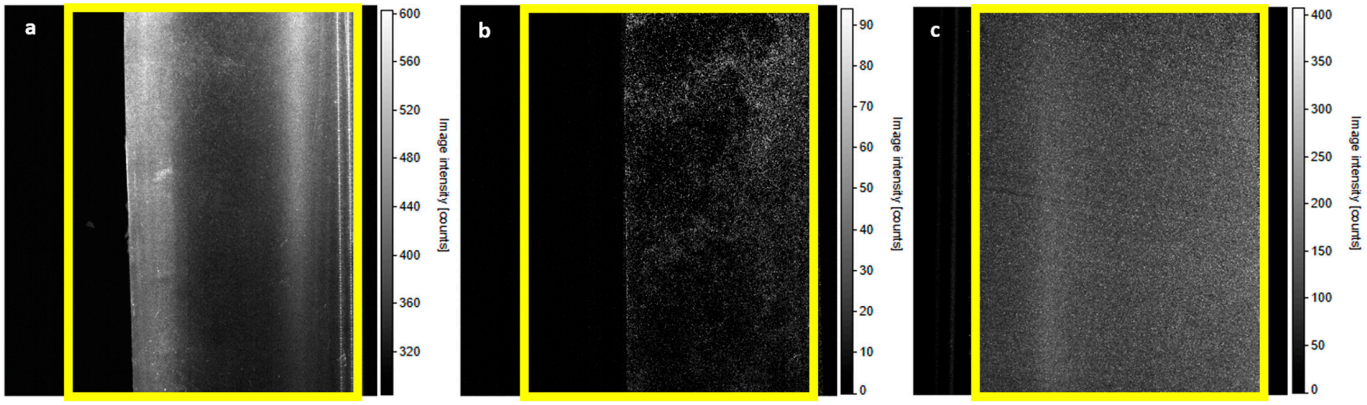


Figure 12. Comparison of intensity maps: (**a**) regime 1, (**b**) regime 2, and (**c**) regime 3.

Table 3. Values of the PPR.

Regime 1	Regime 2	Regime 3
1.55	1.75	1.81

Channel streamlines for regimes 1, 2, and 3 are found in Figure 13. Every regime has a velocity greyscale of up to 9.5 m/s. They are straight and parallel, which is to be expected in this arrangement. However, in regimes 1 and 2, the edge of the shielded part of the profiles is visible on the left side. In regime 2, there are fewer degraded regions than in regime 1 due to background subtraction. Vectors in empty regions were filtered out as erroneous due to high noise. In regime 3, the channel area is completely filled with streamlines.

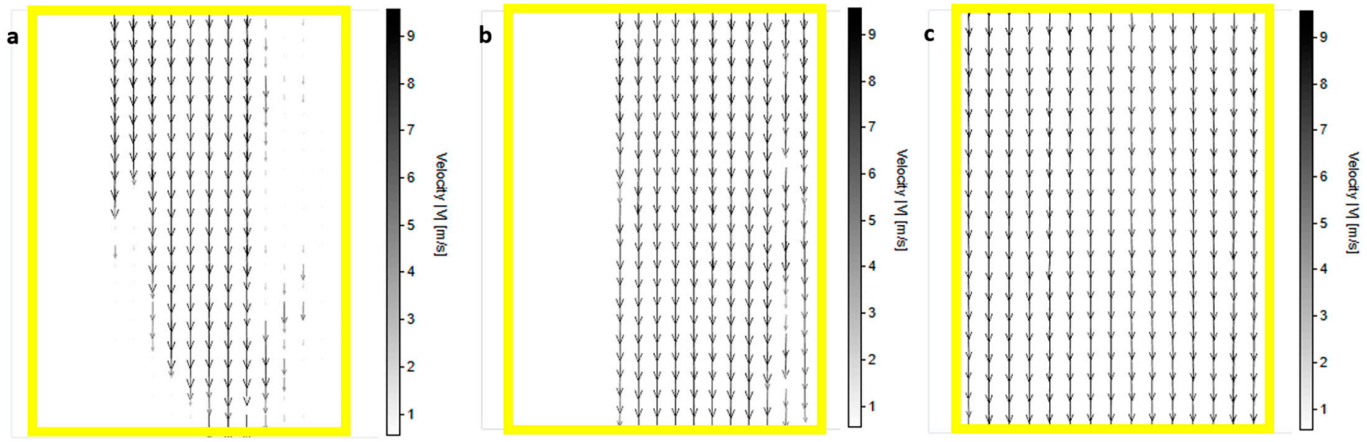


Figure 13. Comparison of measured streamlines: (**a**) regime 1, (**b**) regime 2, and (**c**) regime 3.

The averaged velocity profiles are plotted in the corresponding coordinates in Figure 14 to present the validity of the measured data for each mode. The horizontal primary axis represents the channel diameter in percent. The vertical axis shows the dimensionless velocity relative to the velocity in the middle of the profile. The orange line of regime 1 indicates that this mode is the least suitable as it covers the smallest part of the profile. The blue line of regime 2 is more favorable on the right side. According to the comparison of cases 1 and 2, background subtraction is necessary. However, the data on the left are not available at all due to the shielding. The best is, therefore, the green line of regime 3, i.e., with all modifications. Similar results are represented by the relative measurement uncertainty shown as a dotted line in the corresponding color; the values can be read on the secondary axis. The uncertainty in all three cases increases towards the optically degraded areas. Outside these areas, however, it is always less than 1% of the measured local value.

Dataset 3 is limited only by the vertical red dashed lines that mark the calibrated area. Sections outside this area are invalid due to extreme optical distortion in the peripheral regions of the pipeline. However, this area is 7.4% of the diameter and can be further reduced using a calibration target with a finer marker grid. Still, this work mainly focuses on reducing scattered light inside the measurement space. Therefore, the relevance of the results in close proximity to the wall was not emphasized. Moreover, such a wide area may be sufficient for many potential verification measurements.

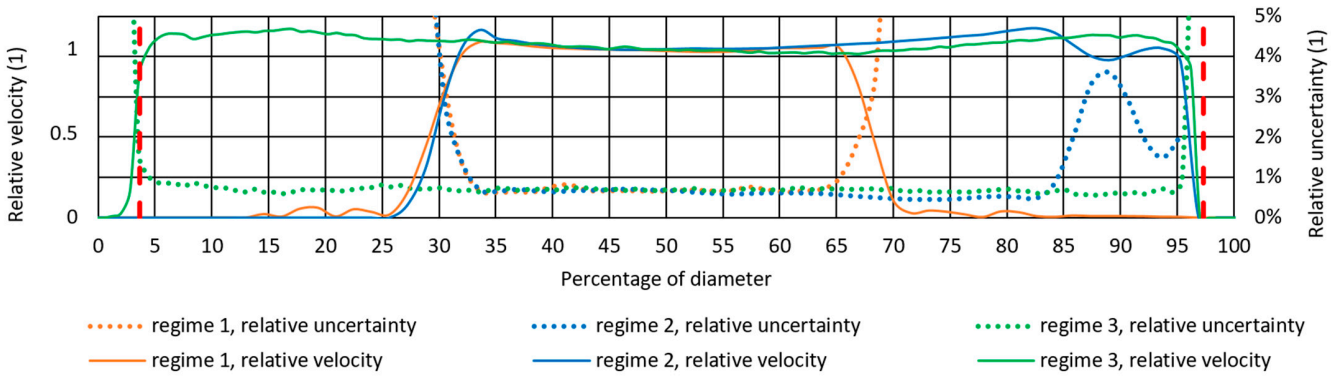


Figure 14. Measurability area for each regime, including relative measurement uncertainty.

7. Conclusions

In this paper, the experimental work focused on the preparation of a cylindrical pipe model for PIV measurements is presented. First, samples were created to find the optimum internal surface modification. The modification chosen was black matt spraying followed by the fluorescent dye spray-based Rhodamine 6G. The tube was surface modified and was also modified geometrically by cutting an elongated gap and inserting a thin flat sheet of plexiglass, which was optically insulated with black sealant from the cylindrical wall to prevent light from spreading through the internal wall structure. Data were measured and compared for the unmodified (default) and modified channels.

Measurements showed that with such a modified pipe, the evaluation could be performed without pre-processing the raw data, i.e., background subtraction. Compared to the unmodified case, no area is degraded by the reflections of direct or scattered light. The only limitation is the extreme distortion on the cylindrical wall close to the walls. The near wall area was 7.4% of the channel diameter but can be reduced using a larger and finer calibration target. In this work, the distortion was corrected only with a standard polynomial calibration model. Advanced distortion avoidance was not investigated in this work and might be a topic for further study. For example, replacing the flow medium with a fluid that has a close refractive index to the pipe material and making a comparison based on similarity theory is suggested. Another possibility is a ray tracing-based image correction method. These algorithms create an artificial image that can significantly reduce high-level distortion. However, this approach may be suitable for higher distortion levels rather than just in the radial direction of the cylindrical channel.

The modifications presented in this paper may also be suitable for possible stereo-PIV measurements in the longitudinal plane of the channel. However, the laser sheet must be wider (approx. 5 or 10 mm), and the gap width must be sufficient for this. This requires further investigation.

Author Contributions: Conceptualization, J.P. and P.D.; methodology, J.P. and J.N.; software, J.P.; validation, J.P., J.N. and P.D.; formal analysis, J.P. and P.D.; investigation, J.P. and J.N.; resources, J.P.; data curation, J.P.; writing—original draft preparation, J.P., P.D. and J.N.; writing—review and editing, J.P., P.D. and J.N.; visualization, J.P.; supervision, P.D.; project administration, P.D.; funding acquisition, J.P. All authors have read and agreed to the published version of the manuscript.

Funding: This work was supported by the Student Grant Competition of the Technical University of Liberec under the project No. SGS-2022-5006.

Data Availability Statement: The data presented in this study are available on request from the corresponding author. The data are not publicly available due to the large size of the raw and evaluated PIV data.

Conflicts of Interest: The funders had no role in the design of the study; in the collection, analyses, or interpretation of data; in the writing of the manuscript; or in the decision to publish the results.

Nomenclature

Symbol	Unit	Description
c_{max}	1	primary peak height
c_2	1	second highest peak height
n	1	refractive index
r	m	radius
PPR	1	primary peak ratio
θ	°, rad	angle
Indexes		
f		reflection
i		incidence
t		refraction
Abbreviations		
DEHS		Di-Ethyl-Hexyl-Sebacat
PIV		particle image velocimetry
SNR		signal-to-noise ratio

References

1. Willert, C.; Gharib, M. Digital Particle Image Velocimetry. *Exp. Fluids* **1991**, *10*, 181–193. [CrossRef]
2. Schröder, A.; Willert, C. (Eds.) *Particle Image Velocimetry "New Developments and Recent Applications"*, 1st ed.; Springer: Berlin/Heidelberg, Germany, 2008. [CrossRef]
3. Prasad, A.; Adrian, R. Stereoscopic particle image velocimetry applied to liquid flows. *Exp. Fluids* **1993**, *15*, 49–60. [CrossRef]
4. Elsinga, G.; Scarano, F.; Wieneke, B.; Oudheusden, B. Tomographic Particle Image Velocimetry. *Exp. Fluids* **2006**, *41*, 933–947. [CrossRef]
5. Xue, Z.; Charonko, J.; Vlachos, P. Particle image velocimetry correlation signal-to-noise ratio metrics and measurement uncertainty quantification. *Meas. Sci. Technol.* **2014**, *25*, 115301. [CrossRef]
6. Paterna, E.; Moonen, P.; Dorer, V.; Carmeliet, J. Mitigation of surface reflection in PIV measurements. *Meas. Sci. Technol.* **2013**, *24*, 057003. [CrossRef]
7. Wieneke, B. *PIV Uncertainty Quantification and Beyond*; Delft University of Technology: Delft, The Netherlands, 2017. [CrossRef]
8. Kumar, B.; Hassebrook, L. Performance Measures for Correlation Filters. *Appl. Opt.* **1990**, *29*, 2997–3006. [CrossRef] [PubMed]
9. Kong, H.J.; Choi, J.; Park, Y.H.; Shin, J.S.; Lee, S.; Lee, D.; Yi, S. Omnidirectional plane beam generation by a hollow tube prism. *Rev. Sci. Instrum.* **2005**, *76*, 026114. [CrossRef]
10. Adatrao, S.; Sciacchitano, A. Elimination of unsteady background reflections in PIV images by anisotropic diffusion. *Meas. Sci. Technol.* **2019**, *30*, aafca9. [CrossRef]
11. Theunissen, R.; Scarano, F.; Riethmuller, M.L. On improvement of PIV image interrogation near stationary interfaces. *Exp. Fluids* **2008**, *45*, 557–572. [CrossRef]
12. Deen, N.; Willems, P.; Annaland, M.; Kuipers, H.; Lammertink, R.; Kemperman, A.; Wessling, M.; Meer, W. On image pre-processing for PIV of single- and two-phase flows over reflecting objects. *Exp. Fluids* **2010**, *49*, 525–530. [CrossRef]
13. Lindken, R. A novel PIV technique for measurements in multi-phase flows and its application to two-phase bubbly flows. *Exp. Fluids* **2002**, *33*, 814–825. [CrossRef]
14. Warjito; Wijaya, E.; Budiarso, B.; Nasution, S.; Kurnianto, M. Study on the Application of Particle Image Velocimetry with Resin and Rhodamine B as Alternative Seeding Particles in Pico Hydro Cross Flow Hydro Turbine. *J. Adv. Res. Fluid Mech. Therm. Sci.* **2021**, *85*, 1–11. [CrossRef]
15. He, L.; Yang, W.; Guan, C.; Yan, H.; Zheng, L.; Zuo, X. Experimental investigation on flow characteristics in circular tube inserted with rotor-assembled strand using PIV. *Chin. J. Chem. Eng.* **2008**, 27. [CrossRef]
16. Wang, Y.; Liu, P.; Shan, F.; Liu, Z.; Liu, W. Effect of longitudinal vortex generator on the heat transfer enhancement of a circular tube. *Appl. Therm. Eng.* **2018**, 148. [CrossRef]
17. Chang, T.-H.; Doh, D.H.; Oh, K. Velocity profiles with swirling flow in a vertical circular tube. *J. Vis.* **2013**, 16. [CrossRef]

18. Depardon, S.; Lasserre, J.; Boueilh, J.; Brizzi, L.; Jacques, B. Skin friction pattern analysis using near-wall PIV. *Exp. Fluids* **2005**, *39*, 805–818. [CrossRef]
19. Bisel, T.; Dahlberg, J.; Martin, T.; Owen, S.; Keanini, R.; Tkacik, P.; Narayan, N.; Goudarzi, N. A Comparison of Flat White Aerosol and Rhodamine (R6G) Fluorescent Paints and Their Effect on the Results of Tomographic PIV Measurements. In Proceedings of the ASME 2017 International Mechanical Engineering Congress and Exposition, Tampa, FL, USA, 3–9 November 2017. [CrossRef]
20. Novosád, J.; Pulec, J.; Dancova, P. Applicability of the PIV system for velocity field measurement inside the ultrasonic flowmeter. *MATEC Web Conf.* **2021**, *345*, 24. [CrossRef]
21. Wangxu, L.; Zhenggui, L.; Wanquan, D.; Zhao, Q.; Lei, J.; Yilong, Q.; Huiyu, C. Particle image velocimetry flowmeter for natural gas applications. *Flow Meas. Instrum.* **2021**, *82*, 102072. [CrossRef]

Disclaimer/Publisher's Note: The statements, opinions and data contained in all publications are solely those of the individual author(s) and contributor(s) and not of MDPI and/or the editor(s). MDPI and/or the editor(s) disclaim responsibility for any injury to people or property resulting from any ideas, methods, instructions or products referred to in the content.